Energy exchange properties during second-harmonic generation in finite one-dimensional photonic band-gap structures with deep gratings

Giuseppe D'Aguanno,[1,2,*] Marco Centini,[1,2] Michael Scalora,[2] Concita Sibilia,[1] Mario Bertolotti,[1] Mark J. Bloemer,[2] and Charles M. Bowden[2]

[1]*INFM at Dipartimento di Energetica, Università di Roma "La Sapienza," Via A. Scarpa 16, I-00161 Rome, Italy*

[2]*Weapons Sciences Directorate, Research Development and Engineering Center, U.S. Army Aviation and Missile Command, Building 7804, Redstone Arsenal, Alabama 35898-5000*

(Received 10 May 2002; revised manuscript received 29 August 2002; published 17 January 2003)

We study second-harmonic generation in finite, one-dimensional, photonic band-gap structures with large index contrast in the regime of pump depletion and global phase-matching conditions. We report a number of surprising results: above a certain input intensity, field dynamics resemble a multiwave mixing process, where backward and forward components compete for the available energy; the pump field is mostly reflected, revealing a type of optical limiting behavior; and second-harmonic generation becomes balanced in both directions, showing unusual saturation effects with increasing pump intensity. This dynamics was unexpected, and it is bound to influence the way one goes about thinking and designing nonlinear frequency conversion devices in a practical way.

DOI: 10.1103/PhysRevE.67.016606 PACS number(s): 42.70.Qs, 42.65.Ky, 42.79.Nv

One of the principal goals in optics is to aquire the basic knowledge necessary to tailor the properties of light. A new class of materials, often referred to as photonic band-gap (PBG) structures, offers this opportunity. These structures are characterized by the existence of allowed and forbidden frequency bands and gaps that either allow or forbid the propagation of light. The analogy to semiconductor band-gap structure was first drawn in the pioneering works of Yablonovitch [1] and John [2] on spontaneous emission control and light localization, which also paved the way for the intense theoretical and experimental investigations that followed. It is impossible to cite the numerous applications proposed over the years. For an up-to-date review of recent advancements in the field, we refer the reader to Ref. [3].

One of the more intriguing uses of one-dimensional (1D) PBG structures that have recently been suggested is their utilization in the realm of quadratic, nonlinear optical interactions as efficient nonlinear frequency converters. However, in the case of second-harmonic generation (SHG), for example, most if not all experimental and theoretical studies have been concerned with the undepleted pump regime [4–8]. The introduction of strong feedback and pump depletion makes the system almost intractable analytically, and to our knowledge it has never been investigated numerically, either. And so we ask: What happens to field dynamics when the regime of pump depletion is approached, under conditions of strong feedback and global phase matching in a finite structure? In addressing this question, we have uncovered a field dynamics that is very much unlike the dynamics that takes place in bulk materials, or any other kind of dynamics that has ever been discussed in the field of nonlinear frequency conversion. We provide surprising answers, and we report that while forward- and backward-propagating components start competing for the available energy initially carried forward by the pump, nonlinear pump reflections overwhelm all other processes, including SHG, leading to a type of optical limiting behavior. Excess pump reflections then lead to saturation of the second harmonic (SH) signal as a function of increasing input pump intensity. This dynamics was unexpected, and it is bound to influence the way one goes about thinking and designing nonlinear frequency conversion devices in a practical way.

In order to study the remarkable dynamics that we have just summarized, we had to come up with a computational method that allowed us to take into account reflections to all orders because feedback and localization play primary roles in gratings with large index contrast. So we begin by writing the scalar nonlinear Helmholtz equations governing the quadratic interactions of two linearly polarized plane waves, one tuned at the fundamental frequency (FF) ω, the other tuned at the SH frequency 2ω, in a layered, 1D, finite, PBG structure:

$$\frac{d^2E_\omega}{dz^2}+\frac{\omega^2\varepsilon_\omega(z)}{c^2}E_\omega=-2\frac{\omega^2}{c^2}d^{(2)}(z)E_\omega^*E_{2\omega}, \tag{1a}$$

$$\frac{d^2E_{2\omega}}{dz^2}+\frac{4\omega^2\varepsilon_{2\omega}(z)}{c^2}E_{2\omega}=-4\frac{\omega^2}{c^2}d^{(2)}(z)E_\omega^2. \tag{1b}$$

$\varepsilon_{j\omega}(z)$ $(j=1,2)$ are the spatially dependent, linear dielectric functions for the FF and SH fields. The condition $\varepsilon_\omega(z)\neq\varepsilon_{2\omega}(z)$ takes into account possible material dispersion. Finally, $d^{(2)}(z)$ is the spatially dependent, quadratic coupling function.

The analysis of Eqs. (1) can be simplified by using a multiple-scale expansion approach [9]. We identify two different spatial scales of variation of the electric fields: (i) a fast scale, which accounts for oscillations that may occur within a spatial scale on the order of the wavelength due to linear interference effects; and (ii) a slow scale, which takes into account the nonlinear polarization source terms on the right-hand sides of Eqs. (1). We now introduce a set of inde-

*Email address: giuseppe.daguanno@uniroma1.it

pendent variables, $z_\alpha=\lambda^\alpha z$ with $\alpha=0,1,2,...$, where λ is a dimensionless parameter that allows fast- and slow-scale variations to be separated. Once the multiple-scales expansion has been performed, the procedure calls for the application of the limit $\lambda\to 1$ to restore the original space variable z. The derivative operator is expanded according to the new variables, namely, $d/dz=\partial/\partial z_0+\lambda\partial/\partial z_1+\lambda^2\partial/\partial z_2+\cdots$. $\varepsilon_{j\omega}(z)$ and $d^{(2)}(z)$ will be considered functions of the fast variable z_0. The electric fields are also expanded in powers of λ in a self-consistent manner: $E_{j\omega}=\lambda E_{j\omega}^{(1)}(z_0,z_1,z_2,\ldots)+\lambda^2 E_{j\omega}^{(2)}(z_0,z_1,z_2,\ldots)+\ldots$, $j=1,2$. Substituting the expansions for the field and the derivative operator into Eqs. (1a, b), and collecting terms proportional to λ, we find that the first-order expansion of the electric fields can be expressed as follows: $E_{j\omega}^{(1)}=A_{j\omega}^{(+)}(z_1,z_2,\ldots)\Phi_{j\omega}^{(+)}(z_0)+A_{j\omega}^{(-)}(z_1,z_2,\ldots)\Phi_{j\omega}^{(-)}(z_0)$, where $\{\Phi_{j\omega}^{(\pm)}\}$ are the left-to-right (LTR, $+$) and right-to-left (RTL, $-$) linear modes that depend only on the fast variable z_0.

We pursue solutions based on LTR and RTL linear modes of the structure, an approach that differs considerably from the usual Bloch mode expansion followed for infinite shallow- or deep-grating structures, where feedback and localization do not occur [10]. These modes can be calculated independently using a standard linear matrix-transfer technique, assuming a unitary electric field is incident on the structure from the left (LTR) or from the right (RTL) [11]. These modes carry information about the linear localization properties of the fields inside the structure. $A_{j\omega}^{(\pm)}(z_1,z_2,\ldots)$ are the field complex amplitudes that depend on the slow variables $(z_1,z_2,\ldots)$. In case there are no nonlinear interactions, $A_{j\omega}^{(\pm)}(z_1,z_2,\ldots)$ are constant amplitudes of LTR and RTL incident fields. Then, collecting terms proportional to λ^2, projecting the resulting equations over the LTR and RTL modes using the standard metric $\langle f|g\rangle\equiv(1/L)\int_0^L f^*(z)g(z)dz$, and taking the limit $\lambda\to 1$ to restore the original spatial variable z, we arrive at four coupled, nonlinear differential equations:

$$\sum_{l=+,-} p_\omega^{(+,l)}\frac{dA_\omega^{(l)}}{dz}=i\frac{\omega}{c}\sum_{(k,l)=(+,-)}\Gamma_{(\omega,+)}^{(k,l)}A_{2\omega}^{(k)}A_\omega^{(l)*}, \tag{2a}$$

$$\sum_{l=+,-} p_\omega^{(-,l)}\frac{dA_\omega^{(l)}}{dz}=i\frac{\omega}{c}\sum_{(k,l)=(+,-)}\Gamma_{(\omega,-)}^{(k,l)}A_{2\omega}^{(k)}A_\omega^{(l)*}, \tag{2b}$$

$$\sum_{l=+,-} p_{2\omega}^{(+,l)}\frac{dA_{2\omega}^{(l)}}{dz}=i\frac{\omega}{c}\sum_{(k,l)=(+,-)}\Gamma_{(2\omega,+)}^{(k,l)}A_\omega^{(k)}A_\omega^{(l)}, \tag{2c}$$

$$\sum_{l=+,-} p_{2\omega}^{(-,l)}\frac{dA_{2\omega}^{(l)}}{dz}=i\frac{\omega}{c}\sum_{(k,l)=(+,-)}\Gamma_{(2\omega,-)}^{(k,l)}A_\omega^{(k)}A_\omega^{(l)}, \tag{2d}$$

where $p_{j\omega}^{(k,l)}=\langle\Phi_{j\omega}^{(k)}|\hat{p}_{j\omega}\Phi_{j\omega}^{(l)}\rangle$, for $j=1,2$ and $k,l=+,-$, $\Gamma_{(\omega,n)}^{(k,l)}=\langle\Phi_\omega^{(n)}|d^{(2)}\Phi_{2\omega}^{(k)}\Phi_\omega^{(l)*}\rangle$, $\Gamma_{(2\omega,n)}^{(k,l)}=\langle\Phi_{2\omega}^{(n)}|d^{(2)}\Phi_\omega^{(k)}\Phi_\omega^{(l)}\rangle$, for $n,k,l=+,-$. $p_{j\omega}^{(k,l)}$ are the matrix elements of the momentum operator $\hat{p}_{j\omega}\equiv -i(c/j\omega)d/dz$, calculated over the RTL and LTR linear modes.

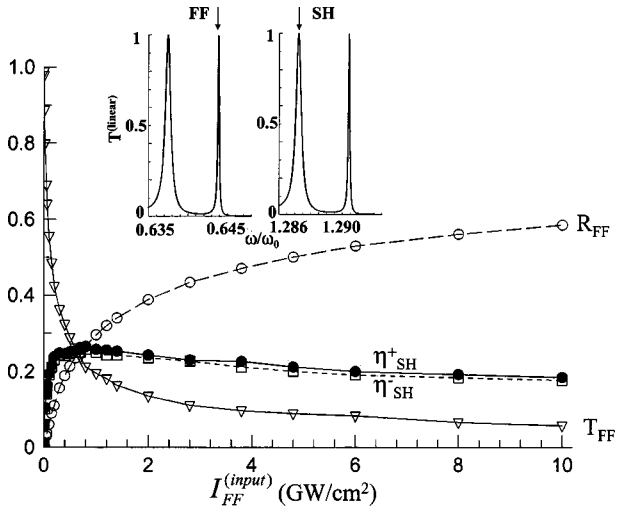

FIG. 1. Forward SH conversion efficiency $\eta_{\rm SH}^{+}=|A_{2\omega}^{(+)}(L)|^2/|A_\omega^{(+)}(0)|^2$ (filled circles, solid line); backward SH conversion efficiency $\eta_{\rm SH}^{-}=|A_{2\omega}^{(-)}(0)|^2/|A_\omega^{(+)}(0)|^2$ (open squares, short dashed line); reflected FF $R_{\rm FF}=|A_\omega^{(-)}(0)|^2/|A_\omega^{(+)}(0)|^2$ (open circles, long dashed line); and transmitted FF $T_{\rm FF}=|A_\omega^{(+)}(L)|^2/|A_\omega^{(+)}(0)|^2$ (open triangles, solid line); vs input FF intensity $I_{\rm FF}^{(\rm input)}=(1/2)\varepsilon_0 c|A_\omega^{(+)}(0)|^2$. The FF intensity is incident from vacuum from LTR. The nonlinear coefficient of the dielectric material is $d^{(2)}=120$ pm/V. The symbols (circles, triangles, and squares) represent the values calculated by numerically integrating Eqs. (2) via a shooting procedure. We note that the total energy in all four channels is conserved, as one might expect: $R_{\rm FF}+T_{\rm FF}+\eta_{\rm SH}^{+}+\eta_{\rm SH}^{-}=1$. Inset: linear transmittance vs normalized frequency ω/ω_0, $\omega_0=2\pi c/\lambda_0$, $\lambda_0=1\,\mu$m. The structure is composed of 59 alternating layers of air and a dielectric material. The index of refraction of the material is $n_H(\omega)=3.342$ at FF ($\lambda\cong 1.55\,\mu$m), and its index of refraction at the SH frequency is $n_H(2\omega)=3.61$. The layers have thicknesses $a=90$ nm (air) and $b=150$ nm (dielectric material), and the total length of the structure is $L=7.11\,\mu$m. The arrows identify tuning of the FF and SH fields, respectively, for global phase-matching operation.

The overlap integrals $\Gamma_{(j\omega,n)}^{(k,l)}$ are effective, complex, coupling coefficients that reflect the way in which the LTR and RTL modes sample the distribution of the nonlinearity $d^{(2)}(z)$ over the structure. Since $\Gamma_{(j\omega,n)}^{(k,l)}$ depend on the amount of overlap between modes, the absolute values can be greater than the magnitude of $d^{(2)}(z)$ when the fields interact coherently inside the structure. Since no assumptions were made regarding the type of grating, Eqs. (2) are valid for arbitrary index profiles and arbitrary tuning conditions, provided the steady-state regime is approached [12]. In all the situations we have analyzed, higher-order contributions give corrections of the order of 10^{-4} with respect to the λ^2 contribution. To summarize, we have numerically integrated our Eqs. (2) using a shooting procedure [13].

As an example, in Fig. 1 we show the reflected and transmitted FF field, the backward and forward SH conversion

efficiencies, as a function of the intensity of the incident FF field, for a PBG structure composed of 59 alternating layers of air, and an ideal, generic, quadratic dielectric material [14]. The details of the structure are described in the figure caption. Layer thicknesses (or lattice constant) are chosen so that the FF field is tuned to the first transmission resonance near the first-order band gap and the SH field is tuned to the second transmission resonance near the second-order band gap (see inset of Fig. 1). Tuning in this fashion, the SH field is globally phase matched with the FF field, as outlined in Ref. [15]. Outside of phase-matching conditions, the SHG process in the PBG structure becomes inefficient and uninteresting [4,7,8].

Several salient points can be pointed out from Fig. 1. (i) The forward and backward SH conversion efficiencies are approximately the same at all times. This is a consequence of the fact that the structure has strong feedback due to the high-index contrast between layers. (ii) Even under global phase matching conditions, SH conversion efficiency does not increase monotonically to deplete the pump, as in bulk materials. We calculate a total maximum conversion efficiency of roughly 50%, approximately equally distributed between the forward and the backward SH channels, for input FF intensities of approximately 0.8 GW/cm^2. We note that the total conversion efficiency tends to saturate in both directions. This behavior is unusual if one thinks just of a phase-matched process and neglects the various components, or channels, that compete for the same available energy. In fact, (iii) the forward FF channel is not only converting energy into SH forward and backward channels, but it is also strongly coupling to the backward FF channel, leading to excess reflections. This is an unexpected result. Therefore, the process of SHG in a PBG structure under conditions of pump depletion should be more appropriately regarded as a multiwave mixing process. Quite surprisingly, the process that is privileged under strong pumping conditions is not SH generation; rather, most of the energy is converted from the FF forward channel to the FF backward channel. The figure suggests that pump reflection exceeds 60% for input intensities of 10 GW/cm^2. (iv) The dynamics outlined above is also strongly suggestive of an unusual optical limiting behavior. Using quadratic interactions for optical limiting purposes would result in faster devices compared with other, more traditional schemes of optical limiters based on cubic nonlinearities (the second-order process utilizes virtual transitions, thus making the process faster). In addition, it would not suffer from the detrimental effects typical of cubic materials such as absorption, heating, or saturation, since energy is always stored in the field and not transferred to the material: our proposed optical limiter would act on the transmitted FF by limiting its energy on the basis of a purely quadratic interaction. It can be shown that for our structure the output FF intensity scales approximately as follows: $I_{\mathrm{FF}}^{\mathrm{output}} \approx a \sqrt{I_{\mathrm{FF}}^{\mathrm{input}}}$ with $a \cong 0.19\ (\mathrm{GW})^{1/2}/\mathrm{cm}$.

The physical mechanism that in this case leads to optical limiting is different than the physical mechanism required for the onset of optical limiting in the case of cubic nonlinearities. In the latter case, optical limiting can occur because of dynamical, spectral band shift in the location of the band gap

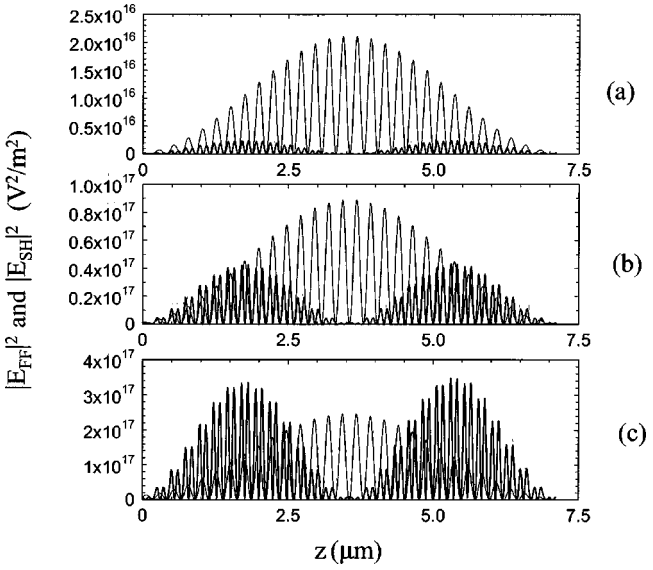

FIG. 2. Absolute value squared of the FF field (thin solid line) and of the SH field (thick solid line) inside the PBG structure, for different values of the input intensity. (a) $I_{\mathrm{FF}}^{(\mathrm{input})} = 0.05$ GW/cm^2. (b) $I_{\mathrm{FF}}^{(\mathrm{input})} = 0.5$ GW/cm^2. (c) $I_{\mathrm{FF}}^{(\mathrm{input})} = 4.8$ GW/cm^2.

[16], and/or in combination with nonlinear absorption. Here, the dynamics is dominated by an energy exchange between the FF forward and the FF backward channels, mediated by the SHG process. To highlight the different mechanisms that drive optical limiting in the case of quadratic and cubic nonlinearities, in Fig. 2 we show the FF and SH field profiles inside the PBG structure during the SHG process for different values of the input intensity. The figures show that the FF remains well localized inside the structure, even when its transmission drops to values less than 10% [Fig. 2(c)]. We do not record any exponentially decaying tails in the FF mode, which are typical of cubic nonlinearities that cause shifts of the band edge and push the FF inside the gap [16]. Finally, the dynamics described in Fig. 1 also suggests another application, namely, a phase-insensitive, nonlinear reflector. In

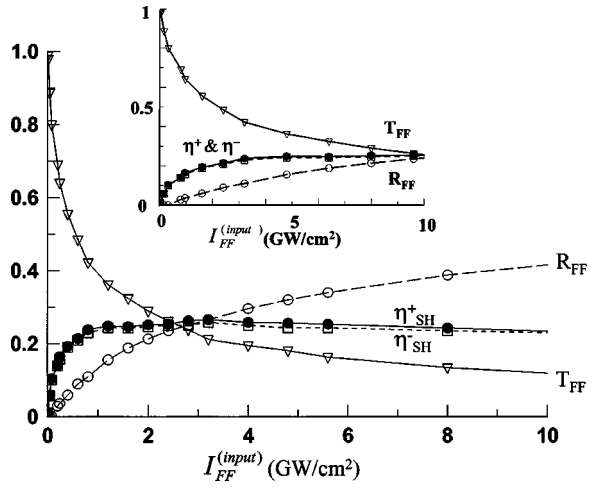

FIG. 3. Same as Fig. 1, but with $d^{(2)} = 60$ pm/V. Inset: same as main figure, but with $d^{(2)} = 30$ pm/V.

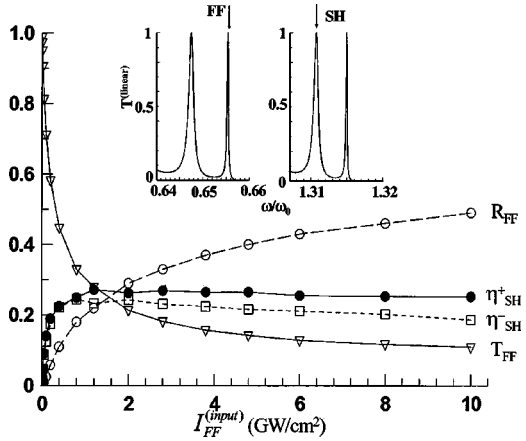

FIG. 4. SH conversion efficiency, reflected and transmitted FF fields vs input FF intensity. The structure is composed of 59 alternating high index/low index layers and it is similar to the one described in Fig. 1, except that low index layers have an index $n_L = 1.5$. Inset: Tuning conditions for global phase-matching operation. The FF is at a wavelength of $\lambda \cong 1.52\ \mu$m.

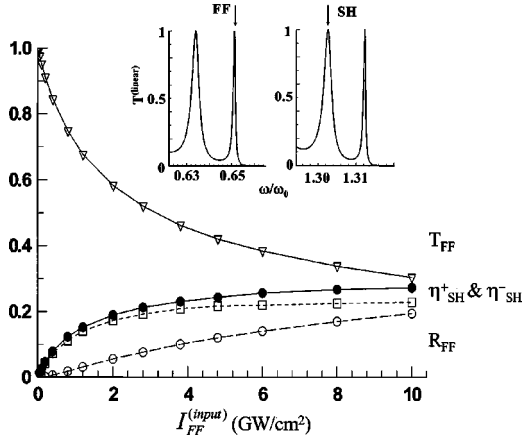

FIG. 5. Same as Fig. 4 However, this structure is composed of 39 alternating high/low index layers. Inset: Tuning conditions for global phase-matching operation. The FF is at a wavelength of $\lambda \cong 1.53\ \mu$m.

our case, the reflection coefficient can be approximately described by the following scaling law: $R_{\mathrm{FF}} \approx b \sqrt[3]{I_{\mathrm{FF}}^{(\mathrm{input})}}$, where $b \cong 0.28\ (\mathrm{cm}^2/\mathrm{GW})^{1/3}$.

In Fig. 3 we show SH conversion efficiencies and reflected and transmitted FF fields for the same structure of Fig. 1, but with different values of the nonlinear coupling coefficient. Comparing Fig. 1 and Fig. 3, we can draw two important conclusions (i) The threshold intensity for the onset of the saturation of the SH conversion efficiency scales approximately as $I_{\mathrm{FF}}^{\mathrm{sat}} \sim (1/d^{(2)})^2$, as one might expect. (ii) The maximum total conversion efficiency available reaches approximately 50% in all the cases studied, regardless of the magnitude of $d^{(2)}$. This limitation is a consequence of the fact that the energy must not only be converted into the SH modes, but also into the FF backward mode. In Fig. 4, we present the results for a structure similar to that of Fig. 1, but with low-index layers with a refractive index of $n_L = 1.5$. We have also studied the case where $n_L = 2.5$, with similar results. The figure suggests that reduction of the index contrast causes the following (i) The backward/forward ratio of the SH conversion efficiencies become unbalanced when the saturation regime is approached: $\eta_{\mathrm{SH}}^{-}/\eta_{\mathrm{SH}}^{+} \cong 1$ for $n_L = 1$ (see Fig. 1), $\eta_{\mathrm{SH}}^{-}/\eta_{\mathrm{SH}}^{+} \cong 0.8$ for $n_L = 1.5$ (see Fig. 4), and $\eta_{\mathrm{SH}}^{-}/\eta_{\mathrm{SH}}^{+} \cong 0.5$ for $n_L = 2.5$, which indicates a scaling law of the type $\eta_{\mathrm{SH}}^{-}/\eta_{\mathrm{SH}}^{+} \sim (\delta n/\bar{n})^{1/2}$, where $\delta n = n_H - n_L$ is the index contrast inside the stack and $\bar{n} = (n_L a + n_H b)/(a+b)$ is the average index of the stack: SH generation in the forward direction becomes privileged. (ii) The threshold pump intensity for the onset of the saturation regime increases: $I_{\mathrm{FF}}^{\mathrm{sat}} \cong 0.8\ \mathrm{GW/cm}^2$ for $n_L = 1$ (see Fig. 1), $I_{\mathrm{FF}}^{\mathrm{sat}} \cong 1.2\ \mathrm{GW/cm}^2$ for $n_L = 1.5$ (see Fig. 4), and $I_{\mathrm{FF}}^{\mathrm{sat}} \cong 10\ \mathrm{GW/cm}^2$ for $n_L = 2.5$. (iii) FF field reflection decreases and FF field transmission increases.

Finally, in Fig. (5) we study the dynamics in a structure similar to the one described in Fig. 4, but composed of only 39 alternating layers. The effects due to the reduction of the number of layers are similar to those already described that come as a result of reducing index contrast: the threshold intensity for the onset of the saturation regime increases, FF field reflection decreases, and FF field transmission increases. The reduction of the number of layers does not substantially affect the backward/forward ratio of SH conversion efficiencies.

Structures almost identical to that described in Fig. 1 have been fabricated using metal organic vapor phase epitaxy (MOVPE) techniques [17]. Structures made by alternating layers of AlGaAs/AlAs have already been used to investigate SHG [7,8] outside of global phase-matching conditions. Very recently, by oxidizing the AlAs layers into AlO_2, Dumeige *et al.* [18] have fabricated several PBG structures composed of 36 and 56 alternating layers of AlGaAs/AlOx, whose indices are approximately 1.5 and 3.4, respectively, operating under global phase-matching conditions in the undepleted pump regime. Therefore, the predictions that we make appear to be quite ready for experimental verification.

In conclusion, for the first time to our knowledge, we have theoretically studied SHG in finite, 1D PBG structures with large index contrast, under conditions of pump depletion and global phase matching. Our results show clear evidence that this process should be more properly regarded as an energy exchange process among four channels; that above a certain value of the input FF intensity the energy exchange between the FF forward and backward channel becomes the privileged process; and that a type of optical limiting based on second-order nonlinearity is obtained.

We thank Nadia Mattiucci, Nicolo Savalli, and Ariel Levenson for helpful discussions. Two of us (G.D. and M.C.) thank the U.S. Army for partial financial support.

[1] E. Yablonovitch, Phys. Rev. Lett. **58**, 2059 (1987).
[2] S. John, Phys. Rev. Lett. **58**, 2486 (1987).
[3] *Nanoscale Linear and Nonlinear Optics*, edited by M. Bertolotti, C. M. Bowden, and C. Sibilia, AIP Conf. Proc. No. 560 (AIP, New York, 2001).
[4] M. Scalora *et al.*, Phys. Rev. A **56**, 3166 (1997).
[5] G. D'Aguanno *et al.*, Opt. Lett. **24**, 1663 (1999).
[6] A. V. Balakin *et al.*, Opt. Lett. **24**, 793 (1999).
[7] Y. Dumeige *et al.*, Appl. Phys. Lett. **78**, 3021 (2001).
[8] G. D'Aguanno *et al.*, Phys. Rev. E **64**, 166091 (2001).
[9] For an extensive review of the multiple-scale expansion approach, the reader can consult A. H. Nayfeh, *Introduction to Perturbation Techniques* (Wiley, New York, 1993).
[10] A. Arraf and C. M. de Sterke, Phys. Rev. E **58**, 7951 (1998), and references therein.
[11] O. Di Stefano, S. Savasta, and R. Girlanda, J. Mod. Opt. **48**, 67 (2001).
[12] The steady-state regime is approached when the interaction time (dwell time) of an input pulse in the PBG structure is much shorter than the duration of the pulse. In the case of transform limited pulses, the spectral bandwidth of the pulse should be much narrower than the spectral bandwidth of each transmission resonance. In the PBG structure we consider (see inset of Fig. 1 for example), the maximum interaction time $\tau_{\mathrm{int}} \approx 1/\Delta\omega_{\mathrm{resonance}}$ at the band edge resonance is approximately 1 ps. For all intents and purposes, input pulses only a few tens of picoseconds in duration can be considered to yield a dynamics in the steady-state regime.
[13] W. H. Press, B. P. Flannery, S. A. Teukolsky, W. T. Vetterling, *Numerical Recipies in C* (Cambridge University Press, Cambridge, England, 1988).
[14] PBG structure made by air/semiconductor material may be obtained by deep etching of waveguides. See, for example, T. F. Krauss and R. M. De La Rue, Prog. Quantum Electron. **23**, 51 (1999), and references therein.
[15] M. Centini *et al.*, Phys. Rev. E **60**, 4891 (1999).
[16] M. Scalora *et al.*, Phys. Rev. Lett. **73**, 1368 (1994).
[17] J. L. Leclercq *et al.*, J. Micromech. Microeng. **10**, 287 (2000).
[18] Y. Dumeige *et al.*, Phys. Rev. Lett. **89**, 043901 (2002), and references therein.